

Correlated electrons tunneling through pseudo Fermi arcs in hyperbolic Fermi surfaces of topological materials

Elena Derunova^{1,7†}, Ángel David Ríos Ortiz², Jacob Gayles³, Yan Sun⁴, Michael W. Gaultois⁵, and Mazhar N. Ali^{6,7}

¹Leibniz Institute for Solid State and Materials Research IFW Dresden, Germany

²Max Planck Institute for Mathematics in the Sciences Leipzig, Germany

³University of South Florida, Tampa, Florida, USA

⁴Max Planck Institute for Chemical Physics of Solids, Dresden, Germany

⁵Leverhulme Research Center for Functional Materials Design, The Materials Innovation Factory, University of Liverpool, Liverpool, UK

⁶Delft University of Technology, Delft, Netherlands

⁷Max Plank Institute of Microstructure Physics, Halle, Germany.

Abstract

In the last few decades, basic ideas of topology have completely transformed the prediction of quantum transport phenomena. Following this trend, we go deeper into the incorporation of modern mathematics into quantum material science focusing on geometry. Here we formulate geometrical conditions of the Fermi surface for a Fermi liquid breakdown and corresponding correlated transport phenomena. As a mechanism to recognize these correlations, we introduce *pseudo Fermi arcs* connecting separate pockets of a hyperbolic Fermi surface. Tunneling through these pseudo arcs and corresponding time-reversal symmetry breaking of purely geometrical origin is referred to as the *Fermi Surface Geometry Effect* (FS-GE). The reliability of the FS-GE is tested on the spin and anomalous Hall effects, traditionally associated with intrinsic time-reversal symmetry breaking. An index, \mathbb{H}_F , quantifying the FS-GE in a particular direction, shows a universal correlation ($R^2 = 0.97$) with the experimentally measured intrinsic anomalous Hall conductivity, of 16 different compounds spanning a wide variety of crystal, chemical, and electronic structure families, including those where topological methods give $R^2 = 0.52$. This raises a question about the predictive limits of topological physics and its transformation into a wider study of bandstructures' and Fermi surfaces' geometries, opening horizon for prediction of phenomena beyond topological understanding.

Main

While the mathematical concept of topology originally arose as a purely theoretical discipline, topological physics exploded onto the scene after the experimental realization of Topological Insulators (TI) [1, 2, 3] in 2007. This opened doors for mathematics mixed with material science to become an important fundamental and technological topic for researching novel physical phenomena as well as technologically relevant properties [2, 4, 5]. The idea of using topological invariants for the classifications of the eigenstates of a Hamiltonian, i.e. electronic bands, has been used to successfully predict protected states and properties including the quantum Hall effects [6, 7]. However, the quantitative prediction of e.g. anomalous (AHE) and spin Hall effects (SHE) in this formalism has had accuracy issues with simple compounds like Ni[8] and fundamentally does not take into account the possible coexistence of multiple *unconnected sets* of bands at the Fermi level, as was recently presented in topological quantum chemistry as multi-EBR bandstructures[9].

The semiclassical transport approach characterizes the energy versus momentum while the idea of analyzing topologically connected eigenstates of the Hamiltonian (i.e. topological bands) results in the formation of quasi-particles and their effect on transport being unable to be simply expressed via the energy gradient in momentum space. It required a different computational paradigm, which is difficult to automate as symmetry, directionality, occupation, and other parameters require careful consideration and processing power. Whilst the major research efforts in the algorithmic quantum transport prediction investigate the optimization of the current computational procedure [10, 11, 9], this manuscript is focused on exploring an alternative way to predict quantum transport directly from ab-initio calculations. For that, we show how manifold theory can give fundamentally different perspectives on topological bands and aid in the prediction of non-trivial quantum transport phenomena in metallic materials.

Manifold theory introduces calculus on multi-valued functions, just like in the case of topological bands (See Section 1 of the supplementary material for a detailed introduction to manifolds). An electronic energy band is, fundamentally, a 3 dimensional(3D), orientable, closed manifold. The theory of these manifolds has been developed over last 100 years by many mathematicians including Thurston [12] and Perelman[13]. This famously led to the proof of the Poincare Conjecture (one of Millennium Prize Problems). According to his work, a 3D manifold, like a band, can be split into regions, where each region can be classified into one of the 8 Thurston geometrical classes. Since the electronic bands fundamentally govern *intrinsic* (not scattering driven) electron transport phenomena in crystalline materials, the geometrical classes must also correspond to intrinsic transport phenomena. This way a *geometrical* understanding of band structures would let one of the most fundamental results in modern mathematics to be applied – not only to condensed matter physics and material science, but also to device technologies.

Developing the complete theory of Electronic Structure Geometry and connecting all

geometrical classes with transport regimes is highly challenging and beyond the authors' current abilities and the scope of this work. Therefore we focus on the hyperbolic class, adding a simplifying assumption, that a band is an *algebraic manifold*. Practically, this means the energy eigenvalues should have a polynomial dependence on momentum, analogous to how in semiclassical formalism the effective mass is expressed as a quadratic polynomial and in bandstructures of real compounds a higher order dependence is sometimes seen. Correspondingly, the Fermi Surface, the constant energy cross-section of the energy-momentum relation is also a manifold, of lower dimension. Using this assumption, we can rephrase two fundamental results from the geometry of algebraic manifolds in theorem 1 and proposition 1; *the hyperbolic geometrical class of the Fermi Surface is linked with the correlated transport phenomena and Fermi liquid breakdown*. As a consequence of this, we will show the existence of *pseudo Fermi arcs* connecting hyperbolic points at separate pockets of the Fermi surface, and correspondingly realize tunneling between those pockets. The pseudo arcs cannot be observed directly like Fermi-arcs in Weyl semimetals and Copper-oxide superconductors (e.g. via ARPES imaging of the Fermi surface), however we show they do result in the breaking of time reversal symmetry and thus have an observable effect on electron transport. Momentum dynamics generated by tunneling through pseudo arcs are referred to as *the Fermi Surface Geometry Effect (FS-GE)*. We demonstrate a numerical application of the FS-GE for the prediction of intrinsic anomalous and spin Hall effects and develop an index, \mathbb{H}_F , for quantifying the FS-GE in the direction of the Hall effect and show that it correlates extremely well with experimentally measured values of intrinsic anomalous Hall conductivity (AHC) ($R^2 = 0.97$, whereas current methods gives just $R^2 = 0.52$). \mathbb{H}_F is tested on 16 different real materials that broadly range from conventional ferromagnets to Weyl semimetals, including cases like Ni and Co_2MnAl , where the Berry phase approach (via the Kubo formalism) does not represent a complete picture of the transport. We found that 13 of the compounds have one EBR FSs (EBR - See Supplement Section 2 for a detailed introduction to EBRs and manifolds) and that the limit of the AHC for a single EBR FS is $\approx 1570 \frac{\hbar}{e}(\Omega\text{cm})^{-1}$. Two of the materials examined here, CrPt_3 and Co_2MnAl , have multi-EBR Fermi surfaces and consequently break that apparent AHC limit. We also find that the FS-GE matches predictions of the spin Hall conductivity (SHC) for Pt, Beta-W, and TaGa_3 . The \mathbb{H}_F index also enables an inexpensive and rapid computational prediction of AHE/SHE materials and can be implemented with existing density functional theory (DFT) methods and databases.

A profound result of this is that modern mathematical concepts can be applied to correlate the geometrical structure of the Fermi surface with non-trivial transport phenomena in a highly diverse set of compounds, proving efficiency of the method. This illustrates the importance of developing a complete theory of *geometrical* understanding for not only Fermi surfaces, but also electronic band structures. This connection between local geometrical properties of the band structure and transport would be a natural extension to the last decade of development in the topological understanding of band structures and transport.

Semicalssical transport and topology

Fundamentally, the Bloch theory of electrons traveling in a periodic potential created by a crystalline lattice allows for the consideration of electron dynamics to be shifted from real space to momentum space (i.e. reciprocal space or k -space) and the Brillouin zone (BZ; the primitive cell in the reciprocal lattice). As is well known, the dynamics of an electron traveling in the crystal potential is then described by the following equations [14]:

$$\hbar \frac{dk_a}{dt} = eE(x) + eH_{ab}(x) \frac{dx^b}{dt} \quad (1)$$

$$\frac{dx^a}{dt} = \frac{1}{\hbar} \frac{\partial}{\partial k_a} \epsilon(k) \quad (2)$$

where $x = (x, y, z)$ is the coordinate of the electron in real space, $k = (k_x, k_y, k_z)$ is momentum, $E(x)$ is an applied electric field, $H(x)$ is an applied magnetic field. From Fermi Liquid Theory, the many-electron dynamics in a crystal potential can be described by the same equations but applied to "quasi-particles" with renormalized dynamical properties as compared to fermions in a Fermi gas [14]. This so-called semiclassical formalism is based on the constant effective mass assumption, i.e. $\frac{\partial^2 \epsilon(k)}{\partial k_a^2} = \text{const.}$ This means $\epsilon(k)$ should be a quadratic function. In a simple one band model it can be approximated with some parameters α, a, γ as following:

$$\epsilon(k) = -\alpha - 4\gamma + \gamma(k_x^2 + k_y^2)a^2 \quad (3)$$

The band structures for real compounds, however, have more than one band and in this case some compounds show the presence of *degenerate* points in the bandstructure, formed by intersections of locally linearly dispersive bands, also known as Dirac or Weyl points. Then equation (2) cannot be applied. A plethora of work in the last two decades has dealt with the ramifications of this, with Dirac/Weyl points resulting in the creation of "Dirac/Weyl quasi-particles". In this case, the quantity called the "Berry curvature" ($\Omega_{ab,n}^c(k)$), is used to quantify the effect of these special points on the transport properties, bringing an additional topological correction to the equation $2 \frac{dx^a}{dt} = \frac{1}{\hbar} \frac{\partial}{\partial k_a} \epsilon(k) + \Omega_{ab,n}^c(k) \frac{dk_b}{dt}$. This represents an electron's orthogonal velocity, as in the AHE (see the supplement for greater detail on this relation) [15, 16, 17, 18].

There are also cases, however, where $\epsilon(k)$ shows cubic or higher order dependence on the momentum k , making the equation 3 not accurate as higher terms can have a significant effect on electrons velocity. Assume, $\epsilon(k)$ is a general polynomial of degree n :

$$\epsilon(k) = P_n(k) = a_n k^n + a_{n-1} k^{n-1} + \dots \quad (4)$$

Replacing equation 2 and finding a simple technique to more generally predict quantum transport in this assumption remains a challenge. It requires different mathematical

approaches and concepts as we show below. In this work we sketch one of the possible methods, however we do not assert that this is the only way.

Fermi surface geometry and anomalous transport

An equation $\epsilon(k) - E_F = 0$ defines a surface in k -space, which separates the occupied and unoccupied states and governs electron transport in metals, and is known as the Fermi surface (FS). For a free electron gas, i.e. when the Hamiltonian has only the kinetic energy term, the FS is a sphere (we denote it as S_F). Naturally, after adding periodic interactions in the Hamiltonian S_F transforms into a 2D surface \tilde{S}_F in k -space. If there exists a smooth transformation from \tilde{S}_F back to S_F , then there is a one to one correspondence between the perturbed state and free electron gas groundstate, so that interacting electrons system can be described via equations 2,1 as in Fermi liquid theory. This is one of the core assumptions of Fermi liquid theory known as the adiabatic continuity approximation. However for a generic surface this smooth transition is not always true, and therefore real materials are known to also show non Fermi liquid behaviors. The phenomena known as "strange metal" phase is observed in unconventional superconductors and quantum Hall materials, among others[19]. To explore this and its connection to the Fermi Surface properties, we need additional mathematical constructions.

Firstly, as it's well known, a 2D surface (e.g. the Fermi surface) can be considered as a Riemannian surface which means for each band forming the FS we can formulate the following theorem:

Theorem 1 *In absence of degenerate points a pocket of the Fermi surface with constant non-positive Gaussian curvature $K \leq 0$ results in the Fermi Liquid breakdown.*

Each pocket of the Fermi surface can be electron or hole type, which means it is an oriented surface (e.g. normal vector towards the Fermi sea for positive orientation). The uniformization theorem can be applied. That means the FS can be transformed to a surface with genus $g \geq 1$ in the condition of the theorem. Since the genus can be understood as the number of holes in the surface, the theorem basically states that if the FS can be transformed to a surface with holes, then it cannot be transformed back to a sphere without shrinking a hole into a point i.e. the adiabatic continuity fails and thus quasiparticles excitation (around a hole) won't behave like non-interacting gas on the S_F . We stress here, that K being non-positive all over the FS is practically a rare case. However, even if some parts of the FS have positive K and some negative, experimental reports show the co-existence of both, Fermi liquid and non Fermi-liquid behaviour within a single FS (e.g. for overdoped cuprates[20, 21]). Therefore similar hypotheses can be made for FSs with varying curvature, which is the more widely realized scenario.

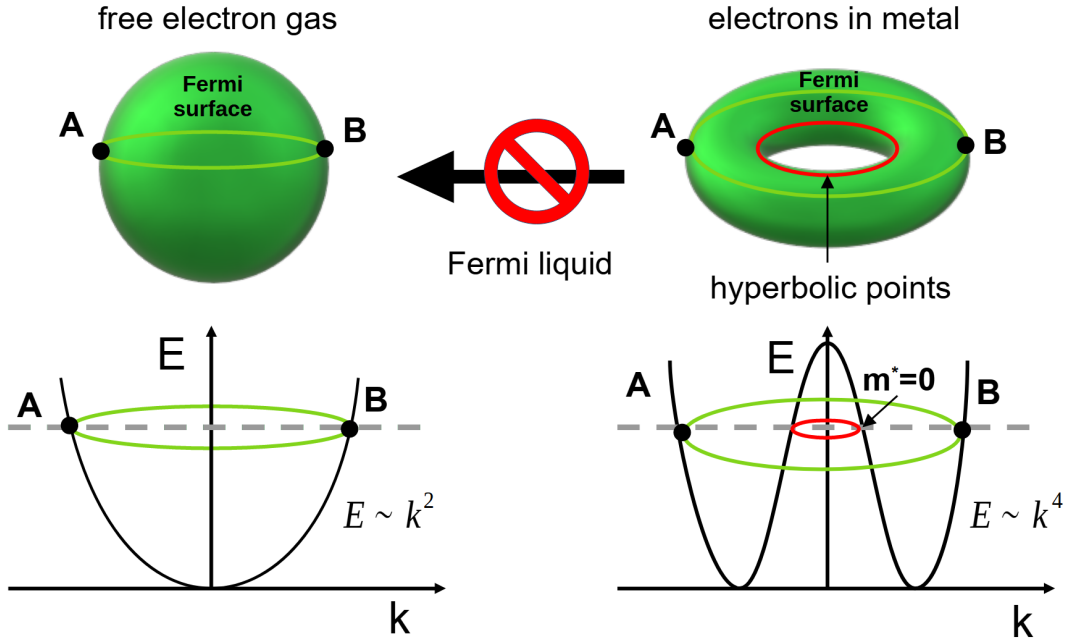


Figure 1: (**color online**): Generation of a hole in the Fermi surface. The left side shows the free electron gas parabolic dispersion and the corresponding Fermi sphere. The right side shows the semimetallic one-band dispersion and generated FS with a hole. The electron and hole pockets are connected along the red circle, where the second derivative of energy changes sign, i.e. the effective mass is zero. This requires the band dispersion to be at least an order of k^4 and the FS has a hole formed by hyperbolic points

In the case of varying Gaussian curvature K , we still can get a surface with $g > 1$. The genus of a surface is connected with the degree of the polynomial describing the surface, i.e. $\text{degree}(\epsilon(k))$.

Lemma 1 *A semi-metallic Fermi surface with non-zero genus and corresponding Fermi liquid breakdown appears only for polynomial dispersion of degree $n > 2$.*

All 2d degree polynomials are well studied and known to not generate a hole, which is consistent with Fermi liquid theory and constant effective mass approximation. Therefore if the FS has holes, the dispersion relation should be polynomial of degree at least 3. For cubic surfaces there are 45 topological types and hole can already appear. For example, a cubic surface with a hole-like feature can be described as $\epsilon(k) = k_z(k_x^2 + k_y^2 - k_z^2 - 1) - 1$ (see details in supplementary). Generally, for $n > 1$ there exists a polynomial $\epsilon(k)$ of degree $2n$ such that FS has n holes as shown in the Appendix. E.g. the dispersion relation $\epsilon(k)$ of the degree 4 generating a hole in the FS can be explicitly written as the following:

$$\epsilon(k) = 2k_y^2 - k_z^2 - 2k_x^2 + k_x^4 + k_y^4 + 2k_x^2k_y^2 \quad (5)$$

This dispersion relation gives a bandstructure similar to the spectrum of the Bogoliubov de-Gennes hamiltonian used for topological superconductors[22, 23] (see figure S8 in the supplement). The Majorana quasi-particles appearing in such topological superconductors don't obey the Fermi liquid behavior. Therefore, a connection between the algebraic structure of the dispersion with the holes in the Fermi surface by the equation 10 is a reasonable starting point for exploring more advanced mechanisms of coupling.

Holes in the Fermi surface are closely related to the change of the effective mass. The generation of a hole is schematically illustrated in figure 1. There must be points (on the red circle in figure 1), where the effective mass changes sign due to the change in sign of the 2nd derivative of the band, which means the effective mass at those points is zero. So massless quasiparticles (like Majorana) and corresponding anomalous transport effects can appear *regardless* Dirac/Weyl points. Geometrically, a hole in the Fermi surface is always made of hyperbolic points ($K \leq 0$). Therefore hyperbolic points making a hole on the FS imply the presence of these "massless points" in the bandstructure and corresponding non-Fermi liquid behavior. However, the "massless points" do not necessarily result into holes in the FS, but can instead result in disconnected pockets. In this case, *the presence of the hyperbolic points remains the signature of "massless points" in the dispersion*(see figure 2 A). For multi-pocket FSs without a hole the Fermi liquid breakdown cannot be derived directly as above and we need further mathematical constructions.

Firstly, an important consideration which needs to be taken into account is the electron's spin, which plays a crucial role in the understanding of anomalous transport effects. Each band (i.e. $\epsilon(k)$ and the FS correspondingly) in the presence of time-reversal symmetry, is doubly degenerate, i.e. occupied with spin up and spin down electrons. To separate them we introduce the complex space \mathbb{C}^3 instead of $\mathbb{R}^3 \times \mathbb{R}^3$, so that momentum of spin up is the real part and momentum of spin down is the imaginary part, e.g. $Z_x = k_x^{up} + i \cdot k_x^{down}$. Assume that no spin interactions were included into the Hamiltonian giving \tilde{S}_F . Then \tilde{S}_F should be localized in the 3D subspace of \mathbb{C}^3 , where $\{Z \in \mathbb{C}^3 : Re(Z_x) = Im(Z_x), Re(Z_y) = Im(Z_y), Re(Z_z) = Im(Z_z)\}$. In this case spin related transport is connected with the FS as following:

Proposition 1 *Hyperbolicity of the spinless FS (i.e. $K < 0$) of a topological semimetal, consisting of more than one pocket, results in spin-correlated transport.*

Spin-correlated transport in this context means a transport regime where electron spins do not behave independently, like e.g. in the spin Hall effect. As we assumed in equation 4, $\epsilon(k)$ is polynomial, thus the FS defined by $\epsilon(k) - E_F = 0$ is an algebraic variety, for the spinful case, as described above, over complex space. Since the FS is semimetallic, it is generated by one EBR according to [9], i.e. by one irreducible representation. Thus the FS is an irreducible algebraic variety over complex space. Therefore the FS must be a connected surface in complex space. That means two pockets of the FS, which actually look separated in reciprocal space are connected in the complex spin-split space. Thus a kind of "tunneling" between two pockets is possible.

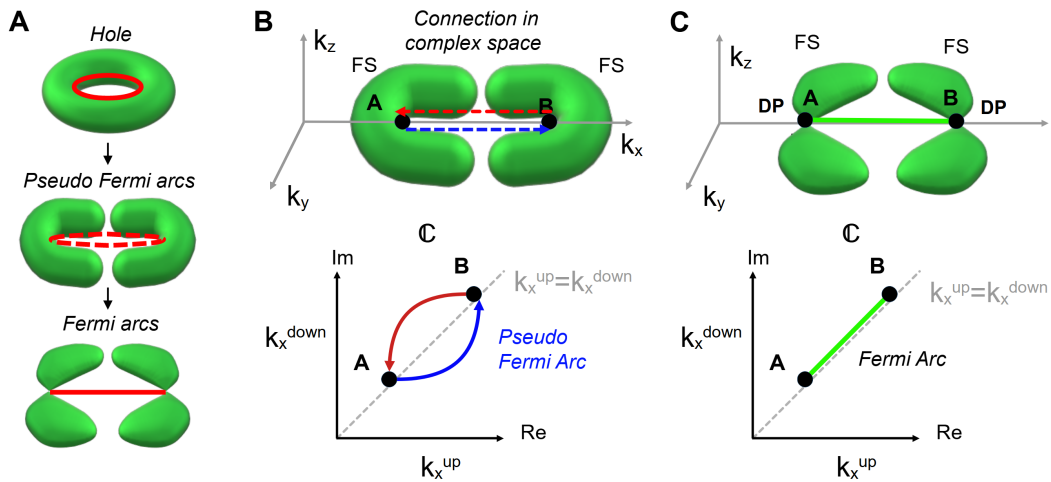


Figure 2: (color online): Schematic diagram of the pseudo Fermi arcs. A. Transition of a single donat-type Fermi surface into separate hyperbolic pockets with the generation of pseudo Fermi arcs and Fermi arcs. B. Top: two hyperbolic pockets of the Fermi surface. Bottom: Fermi arcs (blue and red lines) connecting points on the Fermi surface via complex space. C: Top: two pockets of the Fermi surface with Dirac points (DP) and connecting them Fermi arc. Bottom: Image of the Fermi arc in the complex space

We schematically illustrate this mechanism in figure 2 on the example of tunneling through the k_x direction. Notice, all the points on the FS lay on a diagonal line of the first corner of the complex plane. Assume the pockets cross the k_x axis at points A and B (see figure 2). Connectivity of the FS means there should be a line belonging to the FS and connecting A and B. This line, however, cannot be on the diagonal, because it would have been seen as a part of the FS in the non-complexified k -space. The special case where it is seen, i.e. laying on the diagonal, are regular Fermi arcs [24] as seen in compounds like the high-Tc cuprate superconductors. If we consider the cases where it lays off-diagonal, e.g. below it, then for the points on the line connecting A and B, $k_x^{up} > k_x^{down}$. That demands the breaking of time-reversal symmetry. But as time-reversal symmetry is preserved in the whole, there must be a second inverted "tunnel" above the diagonal, so that $k_1^{up} = k_2^{down}$, $k_2^{up} = k_1^{down}$. So they form a closed loop, similar to a hole, which breaks adiabatic continuity and thus allows non-Fermi liquid behavior and thus electronic correlations. If electrons tunnel in correlated pairs via both channels, in total each momentum will be occupied with both spins and time-reversal symmetry is preserved. In k -space however this is seen just as a swap of momentum between two pockets. This results in a δk , as though a fictional force existed according to the equation 1. However, this force is neither an external force nor Berry curvature (unless the hyperbolic point is a Dirac point as well); these momentum dynamics has a

purely geometrical origin and we refer to it as *Fermi Surface Geometry Effect (FS-GE)*.

Naturally, the FS-GE should result in observable transport properties. The tunneling, described above, happens in opposite directions for each pair, i.e. there is $\delta k_1 = -\delta k_2$. Thus according to the equation 2 there should be two opposite directions of quasiparticle velocities $v_1 = -v_2$. Since they compensate each other and it happens simultaneously, a modulation to the total conductance will not be observed. However, during tunneling, time-reversal symmetry is broken separately for v_1 ($k_x^{up} > k_x^{down}$) and v_2 ($k_x^{up} < k_x^{down}$), thus it should result in time reversal symmetry breaking in two opposite directions, like is observed in the SHE where globally time reversal symmetry is preserved but locally it is broken. Here we stress, that *statically*, in terms of occupancy of the ground state, time reversal symmetry is not broken. The break happens only in the case of momentum *dynamics*, e.g. due to applied E-field.

All the derivations above could have been done without the time-reversal symmetry condition, except for necessity of simultaneous tunneling through both channels. Then, by allowing spin interactions, the single channel works analogously to a Fermi arc connecting two Dirac points on the FS, except it is between the FS pockets, therefore we can talk only about *pseudo-Fermi-arcs* between hyperbolic points. A regular Fermi arc then is a special case of pseudo Fermi arcs, as described above. Then if tunneling happens in one direction, there's just v_1 , which is not compensated. This results in time reversal symmetry breaking and consequently an observed current in the corresponding direction, which is known as the AHE. Notice that in this case, *AHE can be caused purely by the geometry of the band and correspondingly the FS and happen just for a single band at the Fermi level without rising Berry curvature.*

The Berry curvature indicates a connection between topological bands (one EBR bands) manifested via inter-band transition through Dirac/Weyl points, whereas the FS-GE describes the transition mechanism within topologically connected bands away from band-crossing points. A pseudo arc won't appear between two FS pockets from different EBR and therefore band-crossing points at some energies is still a necessary condition for the FS-GE. However, whilst located away from the Fermi level Dirac/Weyl points would still generate Berry curvature contributing to the total AHE in the current computational paradigm, the FS-GE, do not count them, but captures the band geometry, which can come from band crossings or be accidental. Thus there's a possibility to build a computational formalism similar to semiclassical theory and equation 2 but for anomalous velocities, manipulating with normal vectors on the FS of disconnected pockets of one EBR. Then multi-EBR FSs can be just considered as two independent conductive channels, unlike the Berry curvature approach where bands from different EBR are all mixed up.

For real compounds, particular configurations of pseudo arcs and corresponding transport effect is defined by the symmetry of the system and the occupancy of the states. In principle, pseudo arcs are parts of the bands and thus they can be calculated, but, it requires a different approach to the bandstructure calculations. If that's done, the FS-GE could have been numerically estimated, e.g. as $\delta k = \int_{pseudo\ arc} ds$. However,

being technically limited by the conventional DFT calculations, we're not able to test FS-GE directly from the measured properties of the pseudo arc. Instead, we can assume that each hyperbolic point must have such an arc and it is potentially a source of anomalous or spin Hall currents. Indeed, FSs of high SHE/AHE compounds show high concentration of hyperbolic points (see supplementary for the details).

To more rigorously quantify the correlation between hyperbolic points on the FS and AHE/SHE we introduce the index of the concentration of the hyperbolic areas of the FS, which we denote by \mathbb{H}_F and define as the following:

$$\mathbb{H}_F = \sum_{\text{hyperbolic points}} I_n |\sin\alpha| : \sum_{FS} |\sin\alpha| \quad (6)$$

Where α , is an angle between tangent plane to the FS and AHE plane, and I_n is the sign of the $\partial^2\epsilon_n/\partial^2k$ at the BZ boundary in the Hall current direction. As defined, \mathbb{H}_F can have a maximum of "1" which means that the entire FS would be hyperbolic, except for the points where the tangent plane is orthogonal to the AHE plane.

We performed unperturbed DFT calculations of 16 compounds for which intrinsic AHC values were rigorously experimentally determined [25, 26, 27, 28, 29, 30, 31, 32, 33], covering a variety of structural families (perovskites, Heuslers, Kagome lattices, FCC lattices, etc.) and topological classes (Dirac/Weyl/Trivial metals and semimetals). We compared those experimental AHC values to our calculated \mathbb{H}_F (taking care to align the directions of calculation with the directions of measurement for each material in the various experiments). Since, for now, the \mathbb{H}_F parameter is defined for a 2D conductance, we made a comparison of the calculated \mathbb{H}_F with the measured values for thin films or layered structures where the contribution of the third dimension to the total effect is relatively weak.

The result, shown in figure 3, shows an extraordinary linear correlation of the concentration of hyperbolic areas of the FS with the experimentally measured AHC values of all compounds, regardless of structural family or topological class, with an R^2 value of 0.97. Importantly, we also plot the experimentally measured intrinsic AHC values versus the calculated AHC values using the Kubo formalism (based on Berry curvature [25, 29, 28, 30, 31, 8, 32]) for the same compounds (Figure 3d). The R^2 drops down to only 0.52, with a few exceptionally inaccurate cases like Co_2MnAl or Ni , where the error is large and the reason is still under investigation [34]. Even without taking those two compounds into account, the R^2 from the Kubo calculated AHCs only rises to 0.87; significantly worse than the \mathbb{H}_F -dependence. We made a similar calculation for SHE compounds, but due to a paucity of experimental data, we are forced to plot the comparison of the Kubo predicted SHC values for Pt , W_3W [15, 35] and TaGa_3 (See figure S11 in supplement) at different E_F -levels against their corresponding \mathbb{H}_F values in Figure 3b. This graph also shows a strong correlation of the concentration of hyperbolic areas with the Kubo calculated SHCs with an R^2 of about 0.95, implying that the Kubo approach and the FS-GE approach match well in the case of highly uncompensated FS's [36]; a direction of future investigation.

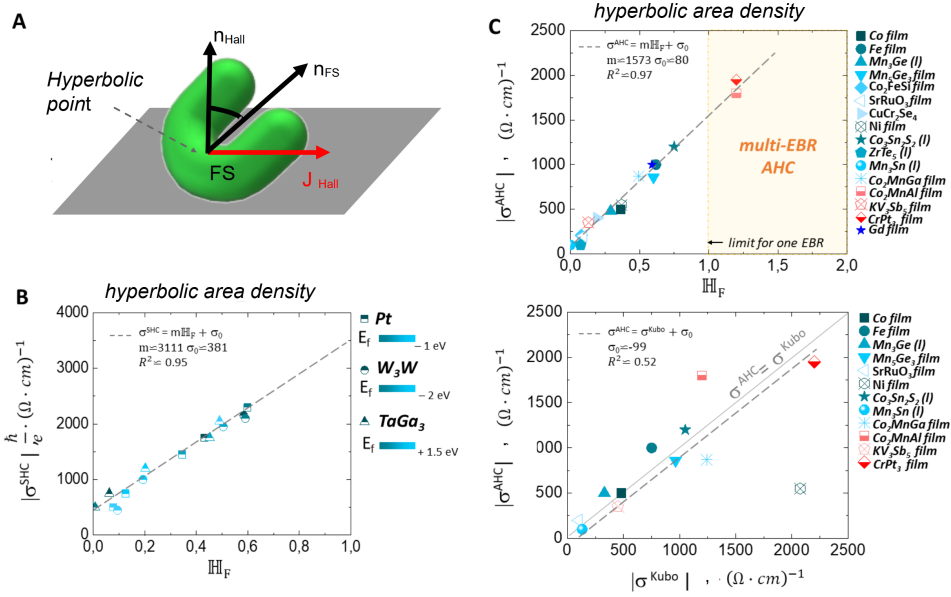


Figure 3: (color online): A. Schematic image of the FS-GE in the direction of Hall measurement. B. Correlation graph of the predicted SHC values via the Kubo formalism vs \mathbb{H}_F , as defined in the text. C. Correlation graph top: *experimentally* determined intrinsic AHC vs \mathbb{H}_F for various materials ((l) identifies layered structures). Bottom: *experimentally* determined intrinsic AHC vs predicted values of AHC via the Kubo formalism.

From the correlation in Figure 3c, it can be seen that in the limit of $\mathbb{H}_F = 1$, the intrinsic AHC is expected to reach a maximum value of $1570 \frac{\hbar}{e} (\Omega \text{cm})^{-1}$. However there are two compounds (Co_2MnAl and CrPt_3) that have \mathbb{H}_F and intrinsic AHCs greater than these maxima. While at first this appears to be an inconsistency, the limit on \mathbb{H}_F can be broken if we take into account the EBR (elementary band representation) for the bands forming FS. Recently it was shown that all bands can be grouped into sets that correspond to distinct EBRs; topological semimetal behavior can be understood as a property of a partially occupied set of such bands (see supplement sections 1 and 2 for more on manifolds and EBRs). Also, the non-quantized contribution to the AHE, as shown by Haldane et al[37], is expected to be a pure Fermi surface property. Combining these two ideas, a part of the FS that is comprised of multiple pockets created by the bands belonging to a single EBR, can be considered distinctly from *another part* of the FS similarly corresponding to the *bands from another EBR*.

In the common case where there is a continuous gap disconnecting sets of bands contributing to the FS, \mathbb{H}_F can be calculated separately using formula 6 for parts of the surfaces arising from distinct sets of bands (bands with differing EBRs), essentially dividing the manifold into submanifolds by EBR, and subsequently summed together in order to characterize the entire FS. This is exactly the case for Co_2MnAl , CrPt_3 and KV_3Sb_5 . For the case of KV_3Sb_5 , it can be seen that the contributions of the

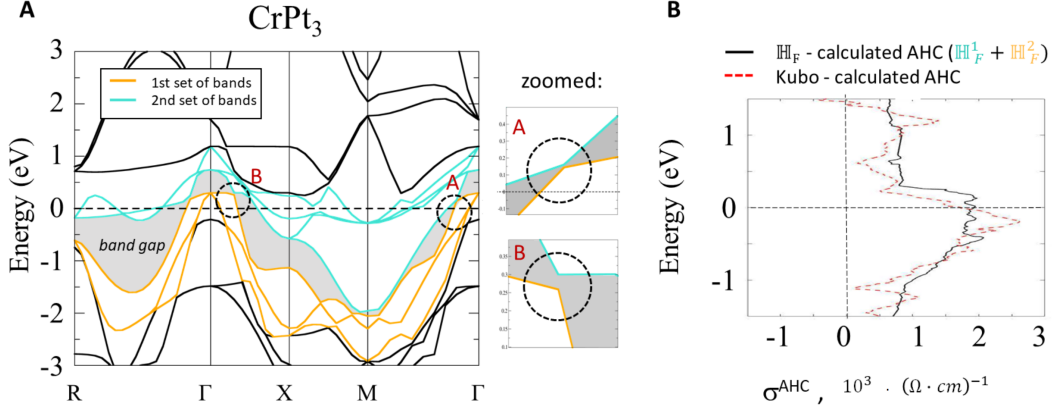


Figure 4: (color online): A. Bandstructure of $CrPt_3$. Blue and yellow colors represent two topologically disconnected (having different EBRs) sets of bands crossing the Fermi level. These sets are disconnected by the continuous gap present between them; i.e. true semimetallic behavior. B. Graph of energy resolved AHC predicted in two different ways: red dashed line is the Kubo based prediction, black dashed line stems from the linear correlation between H_F and AHC calculated separately for FS contributions from each set of bands, then summed together for total H_F .

distinct EBRs are not cooperative, resulting in a relatively low H_F of 0.14. However, for Co_2MnAl and $CrPt_3$, both have cooperative contributions and correspondingly have H_F values larger than 1 as well as AHC values larger than $1570 \frac{\hbar}{e} (\Omega cm)^{-1}$; but they still correlate extremely well with the overall trend in Figure 3c. Figure 4a showcases the detailed bandstructure for $CrPt_3$ with each distinct set of bands colored (blue and yellow) with the continuous gap shaded in gray. The insets clarify the almost-degeneracies near Gamma which are actually gapped. In the Berry curvature approach, the states from the different EBRs are mixed in the total calculation in the Kubo formula. Figure 4 b shows the energy dependent AHC calculated from the Kubo formalism as well as the energy dependent AHC (using the AHC vs H_F correlation $\sigma = mH_F + \sigma_0$ to convert H_F to a numerical AHC value). The results from the two methods are qualitatively similar, but the H_F result has a slightly better quantitative match to experiment.

Discussion

Why does the FS-GE and H_F method appear to fare better than the Kubo approach for these materials and properties? This is a wide area of future investigation, however there are few important considerations we elaborate on here. Firstly, the FS-GE has a different theoretical motivation and can capture something beyond Berry curvature method. Beside that the Kubo formalism looks at the Berry curvature in a point-wise fashion without consideration of their connections to each other, and incorporates a fictitious broadening parameter that does not fully capture finite temperature effects to the electronic structure. Looking at independent points in momentum space means

that if a particular point of importance is missed (because of, for example, a very sharp feature or a too low resolution k -mesh grid), its entire contribution is missed and the calculation can become inaccurate. This is fundamentally different than the *path-wise* FS-GE method which looks at points and their connections to each other because it is approximating trajectories. This is likely related to the \mathbb{H}_F plateaus (S9) at relatively sparse K -meshes of $\approx 30 \times 30 \times 30$, unlike the typical $>150 \times 150 \times 150$ k -mesh grids used in the Kubo analyses (where the k -mesh must also increase for tightening the broadening factor). Secondly, the \mathbb{H}_F calculations rely purely on the first principles calculation of the Fermi Surface and not an interpolated/tight-binding representation of the first principles calculation as in Kubo. This (i) eliminates the need for Wannier/tight-binding Hamiltonians which loses the gauge invariance in the convergence process, and (ii) \mathbb{H}_F calculations are not restrained by the quality of the Wannier fit which are localized functions that will always have trouble capturing the completely de-localized topological states present in some systems. Finally, and perhaps most importantly, the Kubo formalism looks at two-band intersections, not multiband intersections, meaning it ignores higher order intersections that can also result in anomalous transport contribution. The FS-GE method inherently looks at *n-band intersections* since it is a pure Fermi Surface analysis method and the Fermi Surface (and its features) is made up of any number of bands crossing E_F .

When compared with the current Berry curvature driven method for AHE/SHE prediction via the Kubo formalism, the \mathbb{H}_F index is also, computationally, a much simpler metric as it requires just basic DFT calculation without Wannier projection, and thus can be carried out at a significant reduction in time and cost. Importantly, this analysis method can easily be fully automated and implemented into material databases, and can enable artificial intelligence and machine learning based searches of large repositories of compounds for materials with desirable traits for technological applications. For now the \mathbb{H}_F index is still a relatively rough estimation and also is limited to the cases of 2D materials. However, the numerical correlation of the AHE/SHE with \mathbb{H}_F of $R^2 = 0.97$ proves that the concept of using geometric classification is not just a "blue-sky" theoretical research effort; it has immediate applications to outstanding questions in condensed matter physics.

Important future work includes a full derivation of the FS-GE on quasi-particles in reciprocal space and translation into real-space electron transport equations as well as exploring correlations between other geometrical classes of FS regions and other non-fermi liquid transport phenomena. Also, how boundaries between FS regions interact and how they may result into effectively turbulent quasi-particle dynamics. Broadly, the concepts outlined here will alter the current paradigm of understanding the non-trivial transport regimes (like AHE/SHE) moving it to include geometrical properties of the FS, rather than just topological properties of the eigenstates of the Hamiltonian. Suggested complexification of the reciprocal space incorporate spin transport in semiclassical model and connects it with the classification into 8 Thurston geometries. This would be a more complete description of transport properties of crystals, accounting for metals as well as insulators. This way, semi-classical transport equations may be developed using the

idea of a quasi-particle moving along a trajectory described by the geodesic equation of the curved energy-momentum manifold (a bandstructure), rather than a free particle moving with group velocity v_F , *in direct analogy* to the theory of general relativity for a traveler moving along the geodesics of a curved space-time manifold (also a Riemannian manifold where Ricci curvature is used to relate the space-time geometry to the stress-energy tensor). See the supplement for visual demonstration of this analogy (S12).

In summary, we have introduced the general concept of considering the Fermi Surface as a 2D Riemannian manifold and using modern *geometrical classification* to predict non-trivial transport phenomena. We outlined the Fermi Surface Geometry Effect (FS-GE), through the use tunneling between FS points through pseudo Fermi arcs, that relates the concentration of hyperbolic areas of the FS with the anomalous and spin Hall effects. This concept has been applied to develop a simple index, \mathbb{H}_F , for quantifying the contribution of the concentration of hyperbolic areas, and showed a universal correlation ($R^2 = 0.97$) with experimentally measured intrinsic AHE values for 16 different compounds spanning a wide variety of crystal, chemical, and electronic structure families. An apparent maximum value, at $\mathbb{H}_F = 1$, of $1570 \frac{\hbar}{e}(\Omega cm)^{-1}$ was determined for materials with an FS created by bands belonging to a single EBR; materials with multi-EBR FS's can, and do, break this limit as evidenced by CrPt₃ and Co₂MnAl. Use of the \mathbb{H}_F index allows direct calculation of the AHE/SHE at a much lower computational cost than current methods by eliminating the need for Wannier projection and can be implemented with existing high throughput DFT methods and databases. This work highlights the importance of, and opportunities laying ahead for, developing a complete theory of *geometrical understanding* of electronic structure manifolds beginning with Fermi surfaces. Also, these ideas can be extended to bosonic (e.g. magnonic) band structures and their constant energy momentum surfaces as well. In analogy to the broad impact that topological understanding of these structures had, a complete theory of the FS-GE and eventual extension to other dimensional manifolds, will lead to a deeper understanding of at least electron transport and have far reaching consequences in condensed matter physics.

Appendix

The purpose of this short note is to construct smooth algebraic surfaces in \mathbb{R}^3 of any genus. The main idea is to take the so-called lemniscate with n poles in \mathbb{R}^2 , which is an algebraic curve, and then add a quadratic extra parameter together with some small constant in such a way to get an algebraic smooth surface in \mathbb{R}^3 with n holes.

The construction. Let n be a positive integer. If we identify \mathbb{C} with \mathbb{R}^2 , then the complex equation

$$\|Z^n - 1\| - 1 = 0 \tag{7}$$

defines an algebraic curve of degree $2n$ in the variables k_x, k_y in \mathbb{R}^2 .

If $n = 1$, then the complex equation 7 becomes

$$(k_x - 1)^2 + k_y^2 - 1 = 0 \quad (8)$$

which defines a circle in the plane. If $n = 2$ the corresponding equation is

$$(k_x^2 - k_y^2 - 1)^2 + (2k_x k_y)^2 - 1 = 0 \quad (9)$$

also called the lemniscate of Bernoulli.

Let $f_n(k_x, k_y)$ be the polynomial equation 7. By construction, this is a polynomial of degree $2n$ in the variables k_x, k_y . Define the polynomial

$$\varepsilon_n(k_x, k_y, k_z; \delta) = f_n(k_x, k_y)^2 - z^2 - \delta \quad (10)$$

in the variables k_x, k_y, k_z in \mathbb{R}^3 , where $\delta \in \mathbb{R}$ is a constant.

Theorem 2 *For δ small enough the surface X_n , defined as the solutions of the equation $\varepsilon_n(k_x, k_y, k_z, \delta) = 0$, is a smooth surface of genus n in \mathbb{R}^3 .*

A plot of the dispersion relation corresponding to degree 4 can be found in the supplement (figure S8).

Methods

Our calculations have been performed by using the density-functional theory (DFT) with localized atomic orbital basis and the full potential as implemented in the code of full-potential local-orbital (FPLO) [38]. The exchange and correlation energy was considered in the generalized gradient approximation (GGA) level [39]. The electronic band structures were further confirmed by the calculations from *ab-initio* code of WIEN2K [40]. In all the calculations we have used the experimentally measured lattice structures. For the calculation of FS we used 30x30x30 k-meshes, which was found to be a sufficiently dense k-mesh with reasonable computing time (by analysis of the \mathbb{H}_F dependence of k-mesh density for Fe and Co₂FeSi; see Figure S2 for details).

References

- [1] Zhang, H. *et al.* Topological insulators in Bi_2Se_3 , Bi_2Te_3 and Sb_2Te_3 with a single Dirac cone on the surface. *Nature Physics* **5**, 438–442 (2009).
- [2] König, M. *et al.* Quantum Spin Hall Insulator State in HgTe Quantum Wells. *Science* **318**, 766–770 (2007).
- [3] Cercellier, H. *et al.* Evidence for an excitonic insulator phase in 1T-TiSe₂. *Physical review letters* **99**, 146403 (2007).
- [4] Ohno, H., Stiles, M. D. & Dieny, B. Spintronics. *Proceedings of the IEEE. Institute of Electrical and Electronics Engineers* **104**, 1782 (2016).
- [5] Fert, A. Nobel lecture: Origin, development, and future of spintronics. *Rev. Mod. Phys.* **80**, 1517–1530 (2008). URL <https://link.aps.org/doi/10.1103/RevModPhys.80.1517>.
- [6] Liu, C.-C., Feng, W. & Yao, Y. Quantum spin Hall effect in silicene and two-dimensional germanium. *Physical review letters* **107**, 076802 (2011).
- [7] Kane, C. & Mele, E. Quantum spin Hall effect in graphene. *Physical Review Letters* **95**, 226801 (2005).
- [8] Wang, X., Vanderbilt, D., Yates, J. R. & Souza, I. Fermi-surface calculation of the anomalous hall conductivity. *Phys. Rev. B* **76**, 195109 (2007). URL <https://link.aps.org/doi/10.1103/PhysRevB.76.195109>.
- [9] Bradlyn, B. *et al.* Topological quantum chemistry. *Nature* **547**, 298 EP – (2017). URL <http://dx.doi.org/10.1038/nature23268>. Article.
- [10] Tang, e. a. *Comprehensive search for topological materials using symmetry indicators* (Nature, 2019). URL <https://doi.org/10.1038/s41586-019-0937-5>.
- [11] Po, H. C., Vishwanath, A. & Watanabe, H. Symmetry-based indicators of band topology in the 230 space groups. *Nature Communications* **8**, 50 (2017). URL <https://doi.org/10.1038/s41467-017-00133-2>.
- [12] Thurston, W. P. Three dimensional manifolds, kleinian groups and hyperbolic geometry. *Bull. Amer. Math. Soc.* 357–381 (1982).
- [13] Perelman, G. Finite extinction time for the solutions to the ricci flow on certain three-manifolds. *Topologica* **1**, 005 (2008). URL <http://dx.doi.org/10.3731/topologica.1.005>.
- [14] Ashcroft, N. & Mermin, D. *Solid State Physics* (Brooks and Cole, 1976).

- [15] Gradhand, M. *et al.* First-principle calculations of the berry curvature of bloch states for charge and spin transport of electrons. *Journal of Physics: Condensed Matter* **24**, 213202 (2012).
- [16] Tanaka, T. *et al.* Intrinsic spin hall effect and orbital hall effect in 4d and 5d transition metals. *Phys. Rev. B* **77**, 165117 (2008). URL <https://link.aps.org/doi/10.1103/PhysRevB.77.165117>.
- [17] Sinova, J., Valenzuela, S. O., Wunderlich, J., Back, C. H. & Jungwirth, T. Spin hall effects. *Rev. Mod. Phys.* **87**, 1213–1260 (2015). URL <https://link.aps.org/doi/10.1103/RevModPhys.87.1213>.
- [18] Guo, G. Y., Murakami, S., Chen, T.-W. & Nagaosa, N. Intrinsic spin hall effect in platinum: First-principles calculations. *Phys. Rev. Lett.* **100**, 096401 (2008). URL <https://link.aps.org/doi/10.1103/PhysRevLett.100.096401>.
- [19] Stewart, G. Non-fermi-liquid behavior in d-and f-electron metals. *Reviews of modern Physics* **73**, 797 (2001).
- [20] Ray, S. & Das, T. Coexistence of non-fermi liquid and fermi liquid self-energies at all dopings in cuprates. *arXiv preprint arXiv:1703.06280* (2017).
- [21] Chang, J. *et al.* Anisotropic breakdown of fermi liquid quasiparticle excitations in overdoped la₂- x sr x cuo₄. *Nature communications* **4**, 2559 (2013).
- [22] Lado, J. L. & Sigrist, M. Detecting nonunitary multiorbital superconductivity with dirac points at finite energies. *Phys. Rev. Res.* **1**, 033107 (2019). URL <https://link.aps.org/doi/10.1103/PhysRevResearch.1.033107>.
- [23] Aguado, R. Majorana quasiparticles in condensed matter. *La Rivista del Nuovo Cimento* **40**, 523–593 (2017).
- [24] Fang, Y. & Cano, J. Classification of dirac points with higher-order fermi arcs. *Physical Review B* **104** (2021). URL <https://doi.org/10.1103/PhysRevB.104.245101>.
- [25] Liu, E. *et al.* Giant anomalous Hall effect in a ferromagnetic kagome-lattice semimetal. *Nature Physics* **14**, 1125–1131 (2018). URL <https://doi.org/10.1038/s41567-018-0234-5>.
- [26] Miyasato, T. *et al.* Crossover Behavior of the Anomalous Hall Effect and Anomalous Nernst Effect in Itinerant Ferromagnets. *Physical Review Letters* **99** (2007). URL <https://link.aps.org/doi/10.1103/PhysRevLett.99.086602>.
- [27] Nayak, A. K. *et al.* Large anomalous Hall effect driven by a nonvanishing Berry curvature in the noncolinear antiferromagnet Mn₃Ge. *Science Advances* **2**, e1501870 (2016). URL <https://advances.sciencemag.org/lookup/doi/10.1126/sciadv.1501870>.

- [28] Kübler, J. & Felser, C. Weyl Fermions in antiferromagnetic Mn_3Sn and Mn_3Ge . *EPL (Europhysics Letters)* **120**, 47002 (2017). URL <http://arxiv.org/abs/1711.03891>. ArXiv: 1711.03891.
- [29] Zeng, C., Yao, Y., Niu, Q. & Weitering, H. H. Linear Magnetization Dependence of the Intrinsic Anomalous Hall Effect. *Physical Review Letters* **96** (2006). URL <https://link.aps.org/doi/10.1103/PhysRevLett.96.037204>.
- [30] Fang, Z. *et al.* The anomalous hall effect and magnetic monopoles in momentum space. *Science* **302**, 92–95 (2003). URL <https://science.sciencemag.org/content/302/5642/92>. <https://science.sciencemag.org/content/302/5642/92.full.pdf>.
- [31] Imort, I., Thomas, P., Reiss, G. & Thomas, A. Anomalous Hall effect in the Co-based Heusler compounds Co_2FeSi and Co_2FeAl . *Journal of Applied Physics* **111**, 07D313 (2012).
- [32] Tung, J.-C. & Guo, G.-Y. High spin polarization of the anomalous Hall current in Co-based Heusler compounds. *New Journal of Physics* **15**, 033014 (2013). URL <https://iopscience.iop.org/article/10.1088/1367-2630/15/3/033014>.
- [33] Markou, A. *et al.* Thickness dependence of the anomalous hall effect in thin films of the topological semimetal Co_2MnGa . *Phys. Rev. B* **100**, 054422 (2019). URL <https://link.aps.org/doi/10.1103/PhysRevB.100.054422>.
- [34] Ye, L., Tian, Y., Jin, X. & Xiao, D. Temperature dependence of the intrinsic anomalous hall effect in nickel. *Phys. Rev. B* **85**, 220403 (2012). URL <https://link.aps.org/doi/10.1103/PhysRevB.85.220403>.
- [35] Derunova, E. *et al.* Giant intrinsic spin Hall effect in W_3Ta and other A15 superconductors. *Science Advances* **5** (2019). URL <https://advances.sciencemag.org/content/5/4/eaav8575>. <https://advances.sciencemag.org/content/5/4/eaav8575.full.pdf>.
- [36] Hoffmann, A. Spin hall effects in metals. *IEEE Transactions on Magnetics* **49**, 5172–5193 (2013).
- [37] Haldane, F. D. M. Berry Curvature on the Fermi Surface: Anomalous Hall Effect as a Topological Fermi-Liquid Property. *Physical Review Letters* **93** (2004). URL <https://link.aps.org/doi/10.1103/PhysRevLett.93.206602>.
- [38] Koepf, K. & Eschrig, H. Full-potential nonorthogonal local-orbital minimum-basis band-structure scheme. *Phys. Rev. B* **59**, 1743 (1999).
- [39] Perdew, J. P., Burke, K. & Ernzerhof, M. Generalized gradient approximation made simple. *Phys. Rev. Lett.* **77**, 3865 (1996).

- [40] Blaha, P., Schwarz, K., Madsen, G., Kvasnicka, D. & Luitz, J. Wien2k, an augmented plane wave+ local orbitals program for calculating crystal properties. *Technische Universität Wien, Austria* (2001).

This research was supported by the Alexander von Humboldt Foundation Sofia Kovalevskaja Award and the BMBF MINERVA ARCHES Award. E.D. thanks O. Janson and Y. Blanter for the productive discussions and support on this work. M.W.G. thanks the Leverhulme Trust for funding via the Leverhulme Research Centre for Functional Materials Design. All data needed to evaluate the conclusions in the paper are present in the paper and the Supplementary Materials.

Author Contributions E.D. was the lead researcher on this project. She carried out the main theoretical derivations as well as the majority of the DFT calculations and analysis. A.O. assisted mathematical derivations and worked on the construction in the Appendix. M.G. and J.G. assisted with calculations and interpretation. M.N.A and E.D. are the principal investigators.

Competing Interests The authors declare that they have no competing interests.

Correspondence Correspondence and requests for materials should be addressed to Elena Derunova (email: derunova-el@mail.ru).